RSC Advances

PAPER

View Article Online
View Journal | View Issue

Cite this: *RSC Adv.*, 2014, **4**, 17950

Hollow periodic mesoporous organosilicas for highly efficient HIFU-based synergistic therapy†

Xiaoqin Qian,[a] Wenping Wang,*[a] Wentao Kong[a] and Yu Chen*[b]

Nano-biotechnology provides a promising therapeutic strategy for the development of novel cancer therapeutic modalities. In this work, molecularly organic–inorganic hybrid hollow periodic mesoporous organosilicas (HPMOs) were elaborately designed and fabricated by a silica-etching strategy for concurrent high intensity focused ultrasound (HIFU)-based synergistic therapy and combined HIFU-triggered chemotherapy. Due to the unique hollow nanostructures and well-defined spherical morphology, HPMOs themselves have been demonstrated as an efficient synergistic agent to enhance the HIFU ablation efficiency. The well-defined mesoporous shell and large hollow interior can function as the reservoirs for anticancer agents, and the drug (doxorubicin)-releasing exhibits the intelligent on demand profiles under HIFU irradiation due to the specific framework-induced π–π supramolecular stacking between benzene group-bridged framework and doxorubicin molecules. Combined with HIFU ablation and chemotherapy, HPMOs-based intelligent drug delivery nanosystems have demonstrated *in vivo* that anticancer drug-loaded HPMOs can significantly enhance the HIFU therapeutic outcomes due to the combined effects of concurrent enhancement of HIFU ablation and HIFU-triggered chemotherapy. This report gives the first evidence that mesoporous material-based drug delivery nanosystems (*e.g.*, HPMOs) can improve the efficiency of focused ultrasound for cancer surgery, which can be further extended for the development of novel HIFU-based therapeutic modalities for more efficient cancer therapy with mitigated side-effects.

Received 16th December 2013
Accepted 24th February 2014

DOI: 10.1039/c3ra47654e

www.rsc.org/advances

1. Introduction

The development of clinical medicine for the therapy of cancer has raised a new requirement that the tumors should be removed with high efficiency and concurrent low side-effects.[1–6] High intensity focused ultrasound (HIFU) is one of the most effective non-invasive therapeutic modalities by focusing the *in vitro* ultrasound on the *in vivo* lesion tissues to ablate the tumor tissues *via* the thermal, mechanical and cavitation effects.[7,8] However, the therapeutic outcome of HIFU to some tumors within the deep tissues or organs is relatively low due to the limited ultrasound energy deposition within these tumors. The clinical strategy is to increase the ultrasound power to enhance the energy deposition, but it is inevitable that the elevated ultrasound power can cause the severe damage to the normal tissues in the ultrasound-propagation paths.[9] It is highly desirable to develop an efficient technique to increase the HIFU-based therapeutic index with concurrent mitigated side-effects.

Typically, HIFU can ablate and erase the tumors *via* the assistance of outer imaging modalities, such as ultrasound imaging or magnetic resonance imaging.[10,11] However, it is very difficult to remove the tumor tissues completely during the surgical process due to the limited imaging resolution of current therapeutic imaging modalities.[12–16] The remaining tumor tissues or cells may cause the failure of HIFU surgery due to the reoccurrence or the metastasis of cancer cells. The combination of HIFU surgery with other conventional therapeutic modalities, such as chemotherapy, can effectively solve this important issue because the additional chemotherapeutic agents can kill the residual tumor cells to avoid the reoccurrence and metastasis. However, it still remains a big challenge to realize the elaborate combination of HIFU-ablation of tumors with chemotherapy.

In this work, we report, for the first time, a highly efficient strategy for improving the HIFU therapeutic efficiency by using a HIFU-based synergistic agent combined with HIFU-triggered anticancer drug releasing/therapeutic function. Previously, it was reported that nano-biomaterials with either inorganic or organic components could act as the synergistic agent for enhancing the HIFU ablation of tumors by increasing the ultrasound energy deposition within tumor tissues.[17–22]

[a]*The Department of Ultrasound, Zhongshan Hospital, Fudan University, Shanghai 200032, P.R. China. E-mail: puguang61@126.com; Fax: +86-21-64220319; Tel: +86-13681975670*

[b]*State Key Laboratory of High Performance Ceramic and Superfine Microstructures, Shanghai Institute of Ceramics, Chinese Academy of Science, Shanghai 200050, P.R. China. E-mail: chenyu@mail.sic.ac.cn; Fax: +86-21-52413122; Tel: +86-21-52412708*

† Electronic supplementary information (ESI) available. See DOI: 10.1039/c3ra47654e

Especially, the manganese oxide-decorated hollow mesoporous silica nanoparticles (HMSNs) could be used for magnetic resonance imaging-guided HIFU ablation of tumors.[10] However, the traditional inorganic HMSNs suffer from the drawbacks of relatively low biosafety, such as low degradation rates. Comparatively, organic materials-based micro-/nano-particles possess the high biosafety, but their thermal–chemical stability is relatively low.[23] Thus, these organic micro-/nano-particles are easily broken or disintegrated under focused ultrasound with high intensity.[24] It is very promising to fabricate micro-/nano-particles with simultaneous organic and inorganic material-based features for HIFU-based synergistic therapy.[25,26]

Herein, a special type of molecularly organic–inorganic hybrid hollow periodic mesoporous organosilicas (HPMOs) has been elaborately fabricated by silica-etching chemistry for concurrent synergistic HIFU therapy and HIFU-triggered chemotherapy. The first feature of benzene-bridged HPMOs for HIFU therapy is their capability to increase the HIFU energy deposition due to the unique hollow nanostructures. Thus, the HIFU ablation of tumors could be significantly enhanced by using HPMOs as the synergistic agent. Secondly, the well-defined mesoporous shell and large hollow interior can function as the reservoir for the encapsulation of chemotherapeutic agents with high loading capacity.[27–30] Thirdly, the benzene groups within the framework of HPMOs can interact with drug molecules (*e.g.*, doxorubicin) *via* the special π–π interaction, which is very sensitive to ultrasound, and could be triggered by HIFU for intelligent stimuli-responsive drug release. Finally, the organic–inorganic hybrid compositions endow HPMOs with high biocompatibility compared to mostly explored mesoporous silica nanoparticles.[31–33] Therefore, these special HPMOs are anticipated to act as excellent candidate materials for HIFU-based tumor synergistic therapy.

2. Experimental section

Synthesis of HPMOs

Monodispersed HPMOs were fabricated by the following three steps. Firstly, core/shell structured SiO_2@PMOs were prepared by coating a PMOs layer onto the surface of SiO_2 NPs. Typically, ethanol (74 mL), water (10 mL) and ammonia solution (3.14 mL, 36%–38%) were mixed and magnetically stirred in a water bath at 30 °C. Tetraethyl orthosilicate (TEOS, 6 mL) was added into the above solution quickly, and the chemical reaction lasted for another 1 h to form monodispersed silica NPs. Then, the formed silica solution was dropwise added into a solution containing cetyltrimethyl ammonium bromide (CTAB) solution (30 mL, m_{CTAB}: 1.2 g, V_{water}–$V_{ethanol}$ = 1 : 2), ammonia solution (3 mL, 36%–38%) and water (100 mL). After stirring at 30 °C for 30 min, 1,4-bis(triethoxysilyl)benzene (BTEB, 3 mL) was added into the above solution and the reaction lasted for 6 h to form SiO_2@PMOs. The silica core of SiO_2@PMOs were further etched in 0.6 M Na_2CO_3 solution at 80 °C for 1 h. Thirdly, the pore-making agent CTAB was removed by extraction in HCl solution three times at 80 °C, and the products were washed three times by water and ethanol, and finally freeze dried.

DOX-loading into HPMOs

HPMOs (50 mg) were dispersed into DOX PBS solution (0.5 mg mL^{-1}, 20 mL) by mild ultrasound treatment. After stirring for 24 h in the dark, DOX-loaded HPMOs were collected by centrifugation. The obtained products were freeze dried for further use. The supernatant was collected and tested by UV-vis to determine the remaining DOX amount. The DOX content was tested using λ = 480 nm. The DOX loading amount was measured using the following equation: loading amount = (initial DOX amount − DOX amount in supernatant)/(total HPMOs amount + initial DOX amount − DOX amount in supernatant) × 100%. The DOX loading amount is 369 mg g^{-1}.

HIFU-triggered drug release

To investigate the release of DOX from DOX-loaded HPMOs in PBS solution as a result of temperature increase, the DOX–HPMOs were subjected to different temperatures (25, 37, 42 and 60 °C) for up to 60 min using a thermostat-controlled water bath. The released DOX at the exposure temperature was monitored by a UV-vis spectrophotometer.

To systematically investigate the HIFU-triggered drug release, a clinical HIFU system was used, which consists of an ultrasound generator and a single-element transducer placed inside a water bath. The beams of ultrasound were pointed upwards with the sample placed at the focus of the ultrasound. The single-element transducer has an external radius aperture of 120 mm. The dimensions of the focal point are 2 × 2 × 5 mm^3. Pulse wave-HIFU (PW-HIFU) was used in the experiment. DOX-loaded HPMOs (5 mg) were added to a dialysis bag (cut molecular weight: 5000) and then introduced into a vial with PBS (50 mL). Then the dialysis was placed in the focal point. Before and after HIFU irradiation, the medium was removed (5 mL) and replaced with fresh PBS (5 mL). The absorbance intensity of samples was detected by a UV-vis spectrophotometer, and the released DOX in these replaced media was calculated. The temperature at the position of the focal point was measured with a thermocouple. The parameters of PW-HIFU are described as follows: acoustic powers (200 W, 100 W), focal length = 50 mm, continuous emission for 2 s, interval for 1 s, repeat 30 times, total 60 s. Then interval 30 min, repeating the above steps 4 times.

CLSM observations of the uptake of free DOX and DOX–HPMOs, and intracellular release of DOX from DOX–HPMOs

HeLa cancer cells were seeded in the Petri-dishes with one piece of cover glass at the bottom of each well in the incubation medium (DMEM containing 10% FBS, 100 U mL^{-1} ampicillin, 100 μg mL^{-1} streptomycin) and incubated for 24 h at 37 °C. After the medium was removed, DOX–HPMOs dispersed within culture medium (1 mL) were added into the incubation medium at a concentration of 50 μg mL^{-1} for 2 h and 6 h incubation in 5% CO_2 at 37 °C. After the medium was removed, the cells were washed twice with cold PBS (pH = 7.4) and the cover glass was visualized under a laser scanning confocal microscope (Fluo-ViewFV1000, Olympus). Control group containing free DOX

with the same DOX concentration of DOX–HPMOs and culture conditions were employed for the comparisons. The quantitative DOX fluorescent intensities were tested by flow cytometry (FACScan Flow Cytometry, Becton Dickinson, USA).

Ex vivo evaluations of HPMOs-based HIFU synergistic ablation using degassed bovine liver as the model tissue

The effectiveness of HPMOs as the synergistic agent for HIFU-enhanced therapy was evaluated *ex vivo* by choosing the typical degassed bovine liver as the model tissue under the HIFU exposure after the injection of HPMOs in PBS solution (0.3 mL, 6 mg mL^{-1}) or of PBS (0.3 mL) as the control. The real-time ultrasound imaging *ex vivo* was employed to monitor the whole assessment process. When a syringe with the agents was inserted into the bovine liver, the position of the needle tip was monitored by the ultrasound imaging. Immediately after the injection of different agents, HIFU was applied on the injection site with the desired power and time durations (100 W/7 s and 150 W/4 s). The coagulative necrosis could be determined in real-time B-mode ultrasound imaging based on the change of gray scale. After the treatment, the degassed bovine livers were dissected to measure the ablated volume (V). The maximal dimension (length) of lesions was determined according to the z-axis (L), and the width was measured along a perpendicular x-axis (W). The ablated volumes (V [mm^3]) were calculated using the equation of $V = \pi \times L \times W^2/6$.

In vivo therapeutic evaluation of antitumor activity of HIFU-based synergistic therapy combined with chemotherapy

The antitumor activity of HIFU-mediated DOX–HPMOs-treated tumor was evaluated using ICR mice implanted with rat sarcoma S-180. Animal procedures were in agreement with the guidelines of the Institutional Animal Care and Use Committee. Typically, 200 μL of tumor cells (*ca.* 2×10^6) were inoculated at a subcutaneous (s. c.) site in the armpit of right anterior limb of female ICR mice aged 3 weeks. Treatments were started after 2 weeks when the tumors in the mice reached a tumor volume of 10–15 mm^3. Mice were randomly divided into four groups: (i) HIFU group, (ii) DOX–HPMOs group, (iii) DOX–HPMOs + HIFU group and (iv) control group. The number of mice in each group is five. DOX–HPMOs group was injected intratumorally at a dose of 200 μL (the actual dose was 300 μg and DOX concentration was 1.5 mg mL^{-1}). DOX–HPMOs combined with HIFU irradiation (200 W/10 s) group was administrated with the same DOX-equivalent doses combined with HIFU irradiation. The power for HIFU group was 200 W and the duration was 10 s. The control group was only injected with saline solution. Mice were treated weekly for 2 weeks. The treatment effect was assessed by measuring the tumor size every two days. All mice were sacrificed at the end of the test, and the tumor block was separated. Tumor volume was calculated by the formula: $V = 1/2 \times a \times b \times c$, ($a$: the longest diameter, b: the minor diameter and c: the tumor thickness). The inhibition rates of tumor weight and volume were calculated as follows: the inhibition rate of tumor weight% = 1 − [average tumor weigh of experimental group/average tumor weigh of control group] × 100%, the inhibition rate of tumor volume% = 1 − [average tumor volume of experimental group/average tumor volume of control group] × 100%.

Characterizations

Scanning electron microscopy (SEM) and scanning transmission electron microscopy (STEM) were acquired on a field-emission Magellan 400 microscope (FEI Company). Transmission electron microscopy (TEM) was obtained on a JEM-2100F electron microscope operated at 200 kV. The confocal laser scanning microscopy images were recorded in FV1000, Olympus Company. UV-vis spectra were recorded on a UV-3101PC Shimadzu spectroscope. Particle size and Zeta potential was tested on Zetasizer Nano series (Nano ZS90).

3. Results and discussion

The multifunctions of HPMOs for HIFU synergistic therapy are shown in Fig. 1. HPMOs can transport within the blood vessels due to their high dispersity and sub-micrometer size. Then, HPMOs enter the tumor tissues *via* the typical enhanced permeability retention (EPR) effect.[34–36] *In vitro* generated ultrasound can be focused on the tumor tissues based on the tissue penetration capability of ultrasound. The presence of HPMOs with unique hollow structures can change the acoustic environment of tumor tissues to enhance the deposition of ultrasound energy and synergistically improve the HIFU therapeutic efficiency. The drug molecules (doxorubicin, DOX) can be encapsulated within the mesopores and hollow interiors of HPMOs.[37–39] The irritation of HIFU can trigger the release of DOX from the carrier to kill the remaining cancer cells after HIFU ablation. Therefore, HPMOs exhibit two functions for HIFU-based synergistic therapy: enhancing the HIFU ablation outcome and delivering therapeutic agents into tumor tissues.

The synthetic procedure for benzene-bridged HPMOs was based on our previously developed silica-etching chemistry *via* a structure difference-based selective etching mechanism.[25,31,40,41] Firstly, Stöber method-based monodispersed silica nanoparticles (NPs) were coated with a periodic mesoporous organosilica (PMOs) layer to form a special SiO_2@PMOs core/shell

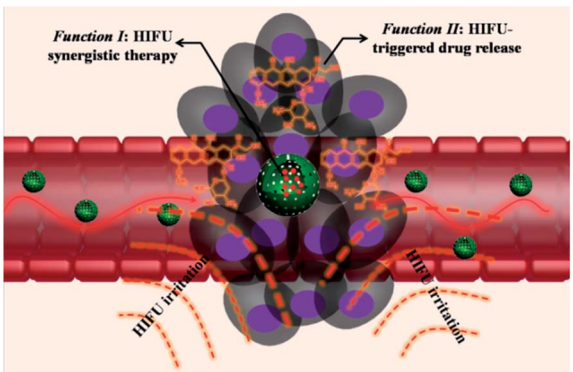

Fig. 1 Schematic illustration of HPMOs-based HIFU synergistic therapy combined with HIFU-triggered drug release.

nanostructure. 1,4-Bis(triethoxysilyl)benzene (BTEB) was employed as the organosilica precursors and cetyltrimethyl ammonium bromide (CTAB) was introduced as the structure-directing agent to form the well-defined mesopores. Then, the solid silica core of SiO_2@PMOs was removed by etching mechanism in mild alkaline solution (0.6 M Na_2CO_3, 80 °C, 1 h) and the CTAB surfactants were extracted in HCl ethanol solution. The microstructures of HPMOs can be easily observed in TEM images (Fig. 2a). It can be found that the obtained HPMOs exhibit the high dispersity without aggregation, which is the prerequisite for further *in vivo* applications to avoid the blocking of blood vessels. The particle size of HPMOs is 450.2 nm (polydispersity index: 0.01),[31] and the Zeta potential is −33.5 mV (Fig. S1†). The hollow nanostructures can be distinguished by the contrast differences in Fig. 2a, and the mesoporous nanostructure can be found in TEM image with high magnification (Fig. S2†). The well-defined mesoporous structures are further demonstrated by small angle X-ray diffraction patterns (Fig. 2b). Both initial core/shell structured SiO_2@PMOs and HPMOs exhibit relatively sharp diffraction peaks between 2–3° in small angle X-ray diffraction patterns, indicating that the formed mesopores are well-ordered to some degree. Compared to the initial SiO_2@PMOs, the peak of HPMOs gives a shift to low-angle position, which indicates that the mesopores are enlarged after the Na_2CO_3 etching process to remove the core. The hollow structure of HPMOs can be further illustrated by dark-field TEM observation (Fig. 2c) where the shell exhibits the bright signals while the interior shows the negative contrast, which is the typical hollow structure-based imaging feature. The well-defined spherical morphology of HPMOs can be found in SEM image (Fig. 2d), which shows that HPMOs exhibit the perfectly spherical shape with smooth surface.

Compared with traditional hollow mesoporous silica nanoparticles (HMSNs) with pure silica composition, benzene-bridged HPMOs show the unique composition-related performances for drug encapsulation and release. As shown in Fig. 3a, the bridged benzene groups are uniformly distributed within

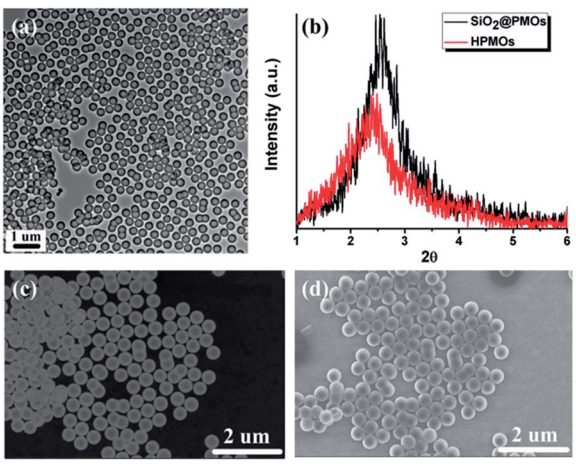

Fig. 2 (a) TEM image of benzene-bridged HPMOs; (b) small angle X-ray diffraction patterns of core/shell structured SiO_2@PMOs and HPMOs; dark-field TEM (c) and SEM (d) images of HPMOs.

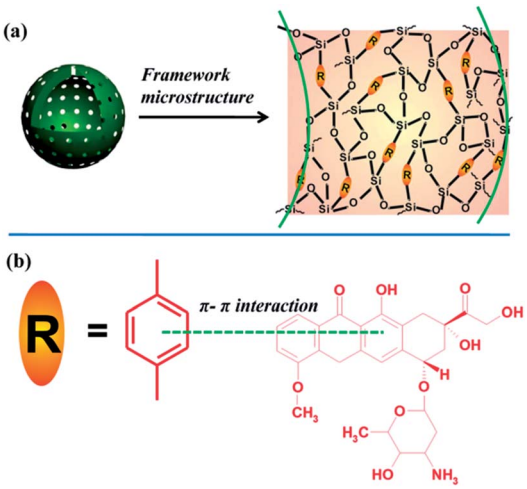

Fig. 3 Schematic microstructural illustration of HPMOs with a molecularly organic–inorganic hybrid framework (a), and the π–π interaction between bridged benzene groups within the framework of HPMOs and DOX molecules (b).

the framework of HPMOs, which provides numerous anchoring points for DOX molecules through supramolecular π–π stacking between benzene groups within the framework of HPMOs and DOX molecules (Fig. 3b). Such non-covalent interaction can keep the drug molecules within the mesopores in physiological conditions while it can be easily disrupted by external triggers, such as focused ultrasound. Based on this mechanism, a novel framework interaction-based stimuli-responsive drug releasing mechanism can be proposed for intelligent on demand drug release.

The intelligent on demand DOX-releasing performance from DOX-loaded HPMOs was evaluated under HIFU irritation with different parameters. It is interesting to find that the DOX releasing exhibits the typical pulsatile profiles under HIFU triggering. The initial release of DOX is slow due to the non-covalent π–π interaction between bridged benzene groups within the framework and DOX molecules. The DOX releasing speeds up once the HIFU irradiation was employed. The releasing percentage can reach 44% (Fig. 4a) and 70% (Fig. 4b) under the condition of 100 W/60 s and 200 W/60 s, respectively. To exclude the temperature effect caused by HIFU triggering, the DOX releasing at different temperatures were tested (25, 37, 42 and 60 °C). It is found that the DOX releasing profiles (Fig. 4c) exhibit the similar patterns at different temperatures, indicating that HIFU-triggered DOX releasing is caused by the mechanical and/or cavitation effect of HIFU rather than the temperature effect. TEM re-test of HPMOs after HIFU exposure shows that the organic–inorganic hybrid framework of HPMOs is very stable under the HIFU irradiation (Fig. 4d and e), demonstrating that the drugs can be released from HPMOs with a sustained manner rather than the explosive release caused by the broken nanospheres. It is noted that focused ultrasound is non-invasive, which also possesses the capabilities of deep-tissue penetration. Therefore, HIFU is regarded as the promising stimuli-responsive trigger for *in vivo* applications.[42,43] In

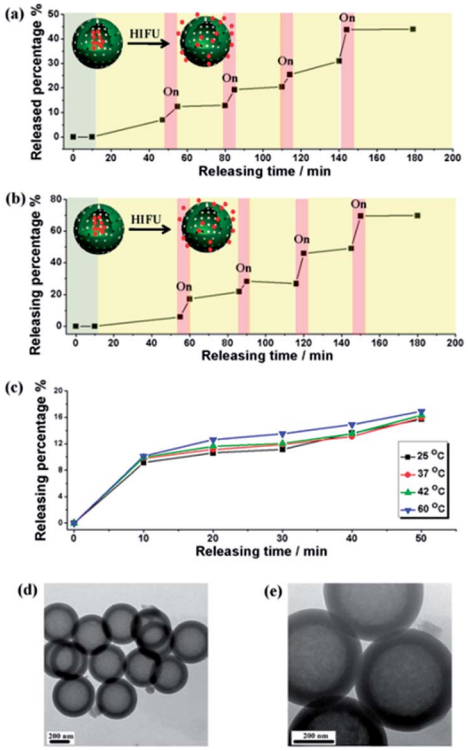

Fig. 4 DOX-releasing from DOX-loaded HPMOs under HIFU irritation with different powers (a: 100 W; b: 200 W); (c) the releasing percentage of DOX from DOX–HPMOs at different temperatures (25, 37, 42 and 60 °C); TEM images of HPMOs with different magnifications (d and e) after HIFU-triggered drug release (200 W).

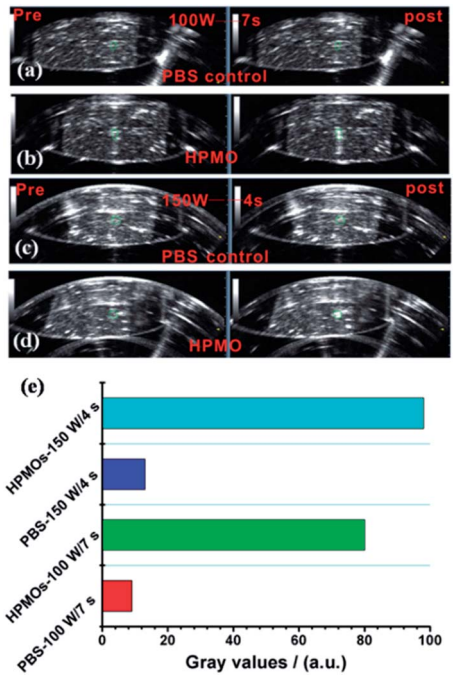

Fig. 5 Typical *in vitro* B-mode ultrasound images before (left column) and after (right column) HIFU exposure on degassed bovine livers at 100 W for 7 s (a: control and b: HPMOs) and 150 W for 4 s (c: control and d: HPMOs); (c) the related gray-scale quantitative values of bovine livers after the HIFU irradiation under different conditions.

addition, the framework-induced intelligent on demand nanosystem is much more favorable for drug delivery compared to traditional nanovalves capped onto the surface of nanopores because the typical nanovalves cover the surface functional groups, which makes the further surface modification difficult.[44–46] Comparatively, the framework-induced stimuli-responsive nanosystem leaves the surface status for further modifications, such as anchoring the targeting moieties or biocompatible polymers. Importantly, such HIFU-triggered drug releasing can circumvent the toxic side-effects of anticancer agents due to its intelligent on demand releasing behaviors, which shows the great clinical application potentials for intelligent drug delivery.

The effectiveness of HPMOs as the synergistic agent for HIFU-enhanced therapy was firstly evaluated *ex vivo* by choosing degassed bovine liver as the typical model tissue after the HIFU exposure under different experimental conditions.[17,21] The real-time ultrasound imaging *ex vivo* was employed to monitor the whole assessment process (Fig. 5a–d). When a syringe with the agents was inserted into the bovine liver, the position of the needle tip was monitored by ultrasound imaging. Immediately after the injection of different agents, HIFU was applied on the injection site with the desired power and time durations (100 W/7 s and 150 W/4 s). The coagulative necrosis could be determined in real-time B-mode ultrasound imaging based on the change of gray scale at the focus (Fig. 5).[21]

It is found that the injection of HPMOs could cause the higher gray value change under either 100 W/7 s or 150 W/4 s compared to the injection of phosphate buffer solution (PBS; *e.g.*, 150 W/4 s: 98 dB for HPMOs and 13 dB for PBS). This result indicates that the introduction of HPMOs can cause higher tissue ablation under HIFU irradiation. To further demonstrate this effect, the bovine liver was dissected for quantitatively calculating the ablated volume. The ablated volume (V) was calculated using the equation $V = \pi \times L \times W^2/6$ where L is the maximal dimension of lesions determined according to the z-axis and W is the width measured along a perpendicular x-axis.[17] As shown in Fig. 6, the HPMOs group exhibits much larger ablated volume of bovine liver than PBS group after the HIFU irradiation. In the group that received HPMOs, the 100 W/7 s HIFU exposure caused the same coagulated volume as the high exposure ultrasound power (150 W/4 s) caused in the group receiving only PBS. This effect is very beneficial for HIFU therapy because the introduced high ultrasound energy could damage the normal tissues in the acoustic propagation channels. The higher necrosis efficiency by HPMOs could be ascribed to the change of acoustic environment of tissues, which enhances ultrasonic energy deposition in tissues and the corresponding intensified mechanical/cavitation effect.[10,17]

As far as the therapeutic efficacy is concerned, HIFU is known to be capable of inducing tissue necrosis by converting ultrasound energy to regional hyperthermia.[7,11,47] However, the energy will rapidly attenuate with penetration depth. Therefore, higher ultrasound energy would be needed to achieve a satisfactory therapeutic effect, which will bring more potential

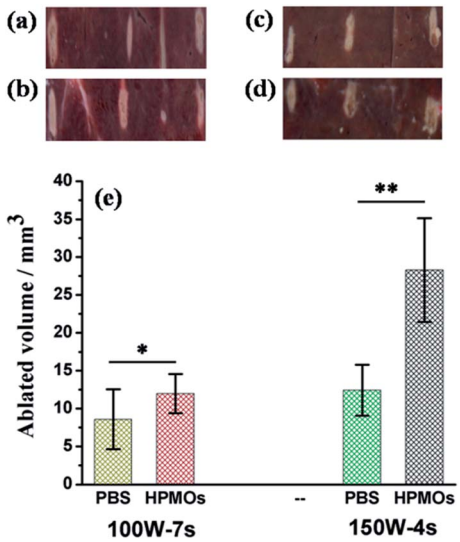

Fig. 6 Digital photos of ablated bovine livers at 100 W for 7 s (a: control and b: HPMOs) and 150 W for 4 s (c: control and d: HPMOs), and the corresponding necrotic volumes (each column is the average of three data; *$P < 0.05$, **$P < 0.01$).

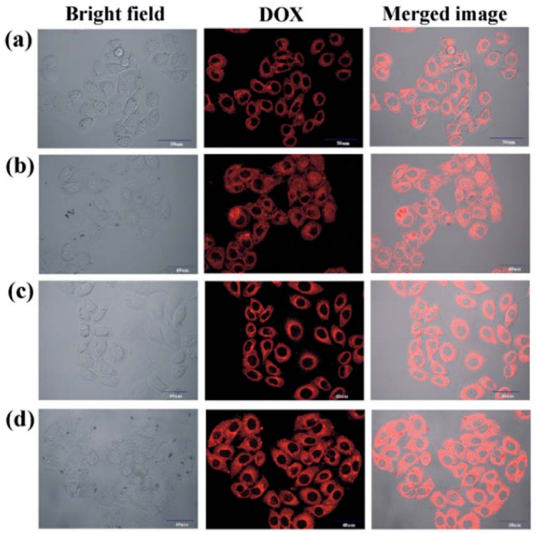

Fig. 7 Confocal laser scanning microscopic (CLSM) images of HeLa cells after co-incubation with free DOX (a and c) and DOX–HPMOs (b and d) for 2 h (a and b) and 6 h (c and d).

dangers to normal tissues. To destroy malignant lesions efficiently, and simultaneously leave neighboring normal tissues unimpaired, HIFU synergistic agents have been strongly recommended to lower the threshold of therapeutic power, position the lesion site, and enhance the final therapeutic efficacy. It has been reported that organic microbubbles or liposomes exhibit an enhancement effect for HIFU therapy.[16,18,20,48–50] However, when exposed to HIFU, the organic-shelled synergistic agent would easily rupture in bolus because of their relatively low strength and low heat-resistance, which is unfavorable for ensuring the necessary circulation and enough imaging time for HIFU operation and post-evaluation. Therefore, substitutes for microbubbles as HIFU therapy synergist are now urgently required. The developed HPMOs with high synergistic efficiency and stability for HIFU therapy provide a new platform for HIFU-based tumor ablation.

In addition to synergistically enhancing the HIFU therapeutic efficiency, the HPMOs can deliver the anticancer agents into cancer cells.[31] The intracellular uptake and release of DOX from DOX-loaded HPMOs were observed by confocal laser scanning microscopy (CLSM). It is found (Fig. 7b and d) that DOX could be effectively delivered within cancer cells (HeLa cell line) mediated by DOX–HPMOs as demonstrated by the presence of strong red fluorescence. Importantly, the fluorescent intensity of HeLa cells after co-incubation with DOX–HPMOs (Fig. 7b and d) is significantly higher than cells after co-incubation with free DOX (Fig. 7a and c), which indicates that more DOX molecules could be delivered into cancer cells *via* HPMOs. Further quantitative determination of the fluorescent intensity by flow cytometry (Fig. S3†) demonstrated that the delivery of DOX mediated by HPMOs could cause a nearly two-fold increase of drug concentrations within the cancer cells after 6 h-incubation. Comparatively, the delivery efficiency of free DOX *via* pass diffusion is much lower. The sustained release of DOX from DOX-loaded HPMOs was demonstrated by the enhancement of fluorescent intensity within cancer cells after 2 h (Fig. 7b) and 6 h (Fig. 7d) co-incubation. The *in vitro* CLSM observations give the direct evidence that DOX-loaded HPMOs can deliver high amounts of DOX molecules into cancer cells with sustained intracellular releasing performances, which guarantee the further HIFU-based ablation and combined chemotherapy.

The *in vivo* antitumor activity of HIFU-mediated tumor ablation combined with chemotherapy was evaluated using ICR mice ($n = 20$) implanted with rat sarcoma S-180 as the animal model and DOX–HPMOs as the concurrent synergistic agent and drug delivery system. Mice were randomly divided into four groups receiving different treatments: (i) HIFU group by using only HIFU irritation (irritation power: 200 W, irritation duration: 10 s); (ii) DOX–HPMOs group; (iii) DOX–HPMOs combined with HIFU (irritation power: 200 W, irritation duration: 10 s) group; and (iv) control group with the administration of saline. The tumor volume was recorded every two days. As shown in Fig. 8, Table 1 and 2, the group of DOX–HPMOs combined with HIFU irritation exhibits the highest antitumor activity compared with control group, DOX–HPMOs group and HIFU group. The antitumor efficiency can reach 80% while the HIFU group and DOX–HPMOs are only 51.10% and 69.22%, respectively. During the experiment, it is found that DOX–HPMOs combined with HIFU irritation could significantly induce the necrosis of tumor tissues due to the combined effects of HIFU ablation, cavitation and DOX molecules-induced cell necrosis. In addition, the unique hollow nanostructures of HPMOs can enhance the ultrasound energy deposition within tumor tissues, and the HIFU can trigger the fast release of therapeutic DOX molecules. Therefore, the combined HPMOs-mediated HIFU synergistic therapy and chemotherapy lead to the highest therapeutic outcome against tumor growth. The histological

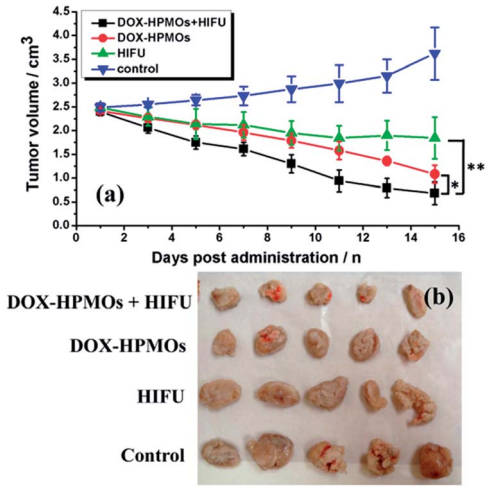

Fig. 8 (a) Changes of tumor volume as a function of time after different treatments (control, HIFU irradiation, DOX–HPMOs and DOX–HPMOs combined with HIFU irradiation, *$P < 0.05$, **$P < 0.01$) in ICR mice implanted with rat sarcoma S-180 ($n = 5$); (b) digital pictures of tumors at the end of therapy under different treatments.

Table 1 The tumor weight and the tumor inhibition rate (IR) for S-180 rat sarcoma treated with different schedules in ICR mice ($n = 5$)[a]

Group	Tumor weight (g)	IR (%)
Control	2.34 ± 0.88	/
HIFU	1.54 ± 0.43$^{(1)}$	34.14
DOX–HPMOs	0.96 ± 0.16$^{(2)}$	59.11
DOX–HPMOs + HIFU	0.63 ± 0.24$^{(3)}$	72.88

[a] *Versus* control group$^{(1)}$ $T = 1.8203$, $P > 0.05$; $^{(2)}$ $T = 3.4550$, $P < 0.01$; $^{(3)}$ $T = 4.1768$, $P < 0.01$. *Versus* (3) group$^{(2)}$ $T = 2.4677$, $P < 0.05$; $^{(1)}$ $T = 4.0840$, $P < 0.01$. *Versus* (1) group$^{(2)}$ $T = 2.8237$, $P < 0.05$.

Table 2 The tumor volume and the tumor inhibition rate (IR) for S-180 rat sarcoma treated with different schedules in ICR mice ($n = 5$)[a]

Group	Tumor volume (cm^3)	IR (%)
Control	3.53 ± 0.65	/
HIFU	1.72 ± 0.77$^{(1)}$	51.10
DOX–HPMOs	1.08 ± 0.19$^{(2)}$	69.22
DOX–HPMOs + HIFU	0.68 ± 0.24$^{(3)}$	80.80

[a] *Versus* control group$^{(1)}$ $T = 3.9684$, $P < 0.01$; $^{(2)}$ $T = 8.0410$, $P < 0.01$; $^{(3)}$ $T = 9.1808$, $P < 0.01$. *Versus* (3) group$^{(2)}$ $T = 3.0381$, $P < 0.05$; $^{(1)}$ $T = 2.2880$, $P < 0.05$. *Versus* (1) group$^{(2)}$ $T = 1.7855$, $P > 0.05$.

observations after TUNEL staining (Fig. 9) show that remarkably destructed cells, large vacuoles and irregular widening of tumor tissues could be found in DOX–HPMOs combined with HIFU irradiation group compared to DOX–HPMOs group, HIFU group and saline control group. It is anticipated that the HPMOs-enhanced HIFU cavitation effect combined with DOX-induced chemotherapy caused such high damage to tumor tissues. The *in vivo* therapeutic outcome indicates that the elaborately designed HPMOs-based nanoplatform provides an excellent

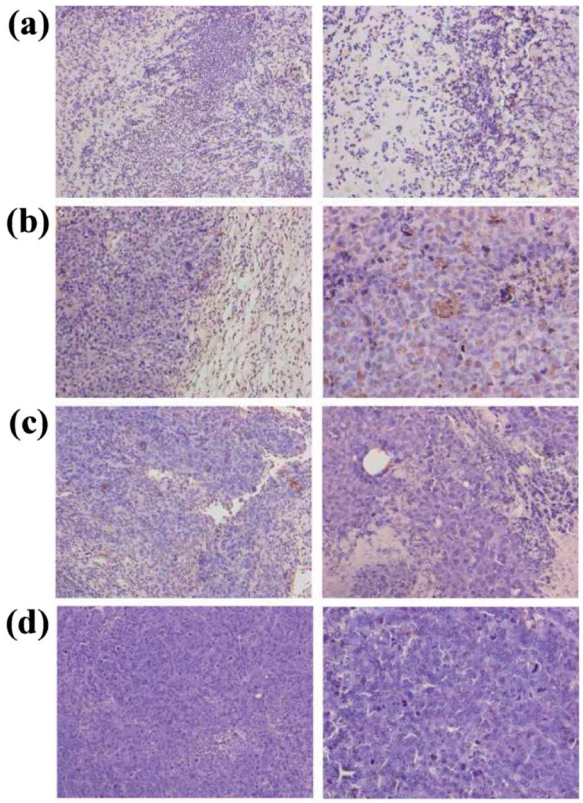

Fig. 9 Histological observations of tumor tissues after different treatments using TUNEL staining (a: DOX–HPMOs combined with HIFU group, b: DOX–HPMOs group, c: HIFU group and d: saline group; magnifications of left images: 200× and right images: 400×).

synergistic agent and intelligent drug delivery nanosystem for highly efficient HIFU-based cancer surgery.

4. Conclusions

In summary, molecularly organic–inorganic hybrid hollow periodic mesoporous organosilicas (HPMOs) were elaborately designed and fabricated for HIFU-based synergistic therapy and combined HIFU-triggered chemotherapy. HPMOs themselves can enhance the HIFU ablation efficiency due to their unique hollow nanostructures to change the acoustic environment of tissues and increase the ultrasound energy deposition. The well-defined mesoporous shell and large hollow interior can function as the reservoirs for anticancer agents, and the drug releasing exhibits the intelligent on demand profiles under HIFU irradiation due to the specific framework-induced π–π supramolecular stacking between benzene group-bridged framework and doxorubicin molecules. The high *in vivo* therapeutic efficiency of HPMOs-enhanced HIFU therapy was also demonstrated against mice xenograft. The introduction of mesoporous material-based drug delivery systems (*e.g.*, HPMOs) provides an alternative therapeutic strategy for highly efficient HIFU-based cancer surgery, which is very promising for further clinical development of novel therapeutic modalities for cancer therapy.

Acknowledgements

This work was supported by the National Nature Science Foundation of China (grant no. 51302293, 81371577), Natural Science Foundation of Shanghai (13ZR1463500) and Foundation for Youth Scholar of State Key Laboratory of High Performance Ceramics and Superfine Microstructures (grant no. SKL201203).

Notes and references

1 V. Wagner, A. Dullaart, A. K. Bock and A. Zweck, *Nat. Biotechnol.*, 2006, **24**, 1211–1217.
2 N. Z. Knezevic, E. Ruiz-Hernandez, W. E. Hennink and M. Vallet-Regi, *RSC Adv.*, 2013, **3**, 9584–9593.
3 T. M. Allen and P. R. Cullis, *Science*, 2004, **303**, 1818–1822.
4 Y. Chen, H. R. Chen and J. L. Shi, *Adv. Mater.*, 2013, **25**, 3144–3176.
5 S. M. Moghimi, A. C. Hunter and J. C. Murray, *FASEB J.*, 2005, **19**, 311–330.
6 X. H. Gao, Y. Y. Cui, R. M. Levenson, L. W. K. Chung and S. M. Nie, *Nat. Biotechnol.*, 2004, **22**, 969–976.
7 M. R. Bailey, V. A. Khokhlova, O. A. Sapozhnikov, S. G. Kargl and L. A. Crum, *Acoust. Phys.*, 2003, **49**, 369–388.
8 P. E. Huber, J. W. Jenne, R. Rastert, I. Simiantonakis, H. P. Sinn, H. J. Strittmatter, D. von Fournier, M. F. Wannenmacher and J. Debus, *Cancer Res.*, 2001, **61**, 8441–8447.
9 J. E. Kennedy, G. R. ter Haar and D. Cranston, *Br. J. Radiol.*, 2003, **76**, 590–599.
10 Y. Chen, H. R. Chen, Y. Sun, Y. Y. Zheng, D. P. Zeng, F. Q. Li, S. J. Zhang, X. Wang, K. Zhang, M. Ma, Q. J. He, L. L. Zhang and J. L. Shi, *Angew. Chem., Int. Ed.*, 2011, **50**, 12505–12509.
11 K. Hynynen, *Ultrasonics*, 2010, **50**, 221–229.
12 J. E. Kennedy, *Nat. Rev. Cancer*, 2005, **5**, 321–327.
13 E. Terreno, F. Uggeri and S. Aime, *J. Controlled Release*, 2012, **161**, 328–337.
14 F. Yang, S. L. Hu, Y. Zhang, X. W. Cai, Y. Huang, F. Wang, S. Wen, G. J. Teng and N. Gu, *Adv. Mater.*, 2012, **24**, 5205–5211.
15 F. Yang, Y. X. Li, Z. P. Chen, Y. Zhang, J. R. Wu and N. Gu, *Biomaterials*, 2009, **30**, 3882–3890.
16 J. A. Feshitan, F. Vlachos, S. R. Sirsi, E. E. Konofagou and M. A. Borden, *Biomaterials*, 2012, **33**, 247–255.
17 X. Wang, H. R. Chen, Y. Chen, M. Ma, K. Zhang, F. Q. Li, Y. Y. Zheng, D. P. Zeng, Q. Wang and J. L. Shi, *Adv. Mater.*, 2012, **24**, 785–791.
18 Y. Zhou, Z. Wang, Y. Chen, H. Shen, Z. Luo, A. Li, Q. Wang, H. Ran, P. Li, W. Song, Z. Yang, H. Chen, Z. Wang, G. Lu and Y. Zheng, *Adv. Mater.*, 2013, **25**, 4123–4130.
19 X. Wang, H. Chen, Y. Zheng, M. Ma, Y. Chen, K. Zhang, D. Zeng and J. Shi, *Biomaterials*, 2013, **34**, 2057–2068.
20 Y. Sun, Y. Y. Zheng, H. T. Ran, Y. Zhou, H. X. Shen, Y. Chen, H. R. Chen, T. M. Krupka, A. Li, P. Li, Z. B. Wang and Z. G. Wang, *Biomaterials*, 2012, **33**, 5854–5864.
21 Y. Chen, Y. Gao, H. R. Chen, D. P. Zeng, Y. P. Li, Y. Y. Zheng, F. Q. Li, X. F. Ji, X. Wang, F. Chen, Q. J. He, L. L. Zhang and J. L. Shi, *Adv. Funct. Mater.*, 2012, **22**, 1586–1597.
22 M. F. Bennewitz, T. L. Lobo, M. K. Nkansah, G. Ulas, G. W. Brudvig and E. M. Shapiro, *ACS Nano*, 2011, **5**, 3438–3446.
23 E. G. Schutt, D. H. Klein, R. M. Mattrey and J. G. Riess, *Angew. Chem., Int. Ed.*, 2003, **42**, 3218–3235.
24 Y. Kaneko, T. Maruyama, K. Takegami, T. Watanabe, H. Mitsui, K. Hanajiri, H. A. Nagawa and Y. Matsumoto, *Eur. J. Radiol.*, 2005, **15**, 1415–1420.
25 Y. Chen, H.-R. Chen and J.-L. Shi, *Acc. Chem. Res.*, 2014, **47**, 125–137.
26 H. T. Ke, J. R. Wang, Z. F. Dai, Y. S. Jin, E. Z. Qu, Z. W. Xing, C. X. Guo, X. L. Yue and J. B. Liu, *Angew. Chem., Int. Ed.*, 2011, **50**, 3017–3021.
27 J. L. Shi, Y. Chen and H. R. Chen, *J. Inorg. Mater.*, 2013, **28**, 1–11.
28 J. E. Lee, N. Lee, T. Kim, J. Kim and T. Hyeon, *Acc. Chem. Res.*, 2011, **44**, 893–902.
29 Y. Chen, C. Chu, Y. C. Zhou, Y. F. Ru, H. R. Chen, F. Chen, Q. J. He, Y. L. Zhang, L. L. Zhang and J. L. Shi, *Small*, 2011, **7**, 2935–2944.
30 Y. Chen, Q. Yin, X. F. Ji, S. J. Zhang, H. R. Chen, Y. Y. Zheng, Y. Sun, H. Y. Qu, Z. Wang, Y. P. Li, X. Wang, K. Zhang, L. L. Zhang and J. L. Shi, *Biomaterials*, 2012, **33**, 7126–7137.
31 Y. Chen, P. Xu, H. Chen, Y. Li, W. Bu, Z. Shu, Y. Li, J. Zhang, L. Zhang, L. Pan, X. Cui, Z. Hua, J. Wang, L. Zhang and J. Shi, *Adv. Mater.*, 2013, **25**, 3100–3105.
32 H. Djojoputro, X. F. Zhou, S. Z. Qiao, L. Z. Wang, C. Z. Yu and G. Q. Lu, *J. Am. Chem. Soc.*, 2006, **128**, 6320–6321.
33 C. Urata, H. Yamada, R. Wakabayashi, Y. Aoyama, S. Hirosawa, S. Arai, S. Takeoka, Y. Yamauchi and K. Kuroda, *J. Am. Chem. Soc.*, 2011, **133**, 8102–8105.
34 B. E. Oeffinger and M. A. Wheatley, *Ultrasonics*, 2004, **42**, 343–347.
35 H. Hu, H. Zhou, J. Du, Z. Q. Wang, L. An, H. Yang, F. H. Li, H. X. Wu and S. P. Yang, *J. Mater. Chem.*, 2011, **21**, 6576–6583.
36 H. P. Martinez, Y. Kono, S. L. Blair, S. Sandoval, J. Wang-Rodriguez, R. F. Mattrey, A. C. Kummel and W. C. Trogler, *MedChemComm*, 2010, **1**, 266–270.
37 L. L. Li, Y. Q. Guan, H. Y. Liu, N. J. Hao, T. L. Liu, X. W. Meng, C. H. Fu, Y. Z. Li, Q. L. Qu, Y. G. Zhang, S. Y. Ji, L. Chen, D. Chen and F. Q. Tang, *ACS Nano*, 2011, **5**, 7462–7470.
38 H. Meng, M. Xue, T. Xia, Z. X. Ji, D. Y. Tarn, J. I. Zink and A. E. Nel, *ACS Nano*, 2011, **5**, 4131–4144.
39 Z. G. Feng, Y. S. Li, D. C. Niu, L. Li, W. R. Zhao, H. R. Chen, L. Li, J. H. Gao, M. L. Ruan and J. L. Shi, *Chem. Commun.*, 2008, 2629–2631.
40 Y. Chen, H. R. Chen, L. M. Guo, Q. J. He, F. Chen, J. Zhou, J. W. Feng and J. L. Shi, *ACS Nano*, 2010, **4**, 529–539.
41 Y. Chen, H. R. Chen, D. P. Zeng, Y. B. Tian, F. Chen, J. W. Feng and J. L. Shi, *ACS Nano*, 2010, **4**, 6001–6013.
42 C. Oerlemans, R. Deckers, G. Storm, W. E. Hennink and J. F. W. Nijsen, *J. Controlled Release*, 2013, **168**, 327–333.

43 G. D. Moon, S. W. Choi, X. Cai, W. Y. Li, E. C. Cho, U. Jeong, L. V. Wang and Y. N. Xia, *J. Am. Chem. Soc.*, 2011, **133**, 4762–4765.
44 C. Park, H. Kim, S. Kim and C. Kim, *J. Am. Chem. Soc.*, 2009, **131**, 16614–16615.
45 D. R. Radu, C. Y. Lai, K. Jeftinija, E. W. Rowe, S. Jeftinija and V. S. Y. Lin, *J. Am. Chem. Soc.*, 2004, **126**, 13216–13217.
46 Y. F. Zhu, J. L. Shi, W. H. Shen, X. P. Dong, J. W. Feng, M. L. Ruan and Y. S. Li, *Angew. Chem., Int. Ed.*, 2005, **44**, 5083–5087.
47 A. C. Schmitz, D. Gianfelice, B. L. Daniel, W. Mali and M. van den Bosch, *Eur. J. Radiol.*, 2008, **18**, 1431–1441.
48 J. W. Huang, J. S. Xu and R. X. Xu, *Biomaterials*, 2010, **31**, 1278–1286.
49 E. Kang, H. S. Min, J. Lee, M. H. Han, H. J. Ahn, I. C. Yoon, K. Choi, K. Kim, K. Park and I. C. Kwon, *Angew. Chem., Int. Ed.*, 2010, **49**, 524–528.
50 E. Huynh, J. F. Lovell, B. L. Helfield, M. Jeon, C. Kim, D. E. Goertz, B. C. Wilson and G. Zheng, *J. Am. Chem. Soc.*, 2012, **134**, 16464–16467.